University of Pennsylvania
ScholarlyCommons

Departmental Papers (MSE) Department of Materials Science & Engineering

June 2006

Defects in GaN Nanowires

Douglas Tham
University of Pennsylvania

Chang-Yong Nam
University of Pennsylvania

John E. Fischer
University of Pennsylvania, fischer@seas.upenn.edu

Follow this and additional works at: http://repository.upenn.edu/mse_papers

Recommended Citation

Tham, D., Nam, C., & Fischer, J. E. (2006). Defects in GaN Nanowires. Retrieved from http://repository.upenn.edu/mse_papers/114

Postprint version. Published in *Advanced Functional Materials*, Volume 16, Issue 9, June 2006, pages 1197-1202.
Publisher URL: http://www3.interscience.wiley.com/cgi-bin/jhome/77003362

This paper is posted at ScholarlyCommons. http://repository.upenn.edu/mse_papers/114
For more information, please contact libraryrepository@pobox.upenn.edu.

Defects in GaN Nanowires

Abstract
High resolution and cross-sectional transmission electron microscopy (HRTEM, XTEM) were used to characterize common defects in wurtzite GaN nanowires grown via the vapor-liquid-solid (VLS) mechanism. High resolution transmission electron microscopy showed that these nanowires contained numerous (001) stacking defects interspersed with cubic intergrowths. Using cross-sectional transmission electron microscopy, bicrystalline nanowires were discovered with two-fold rotational twin axes along their growth directions, and were concluded to grow along high index directions or vicinal to low index planes. A defect-mediated VLS growth model was used to account for the prevalence of these extended defects. Implications for nanowire growth kinetics and device behavior are discussed.

Comments
Postprint version. Published in *Advanced Functional Materials*, Volume 16, Issue 9, June 2006, pages 1197-1202.
Publisher URL: http://www3.interscience.wiley.com/cgi-bin/jhome/77003362

This journal article is available at ScholarlyCommons: http://repository.upenn.edu/mse_papers/114

Defects in GaN Nanowires**

By *Douglas Tham, Chang-Yong Nam and John E. Fischer*[*]

[*] D. Tham, C. Y. Nam, Prof. J. E. Fischer

Department of Materials Science and Engineering, University of Pennsylvania,

3231 Walnut Street, Philadelphia, Pennsylvania 19104-6272

E-mail address: fischer@seas.upenn.edu

[**] This research was supported by the US Department of Energy Grant DE-FG02-98ER45701. The use of shared facilities supported by Penn's NSF/MRSEC under Grant DMR02-03378 is gratefully acknowledged.

TABLE OF CONTENTS

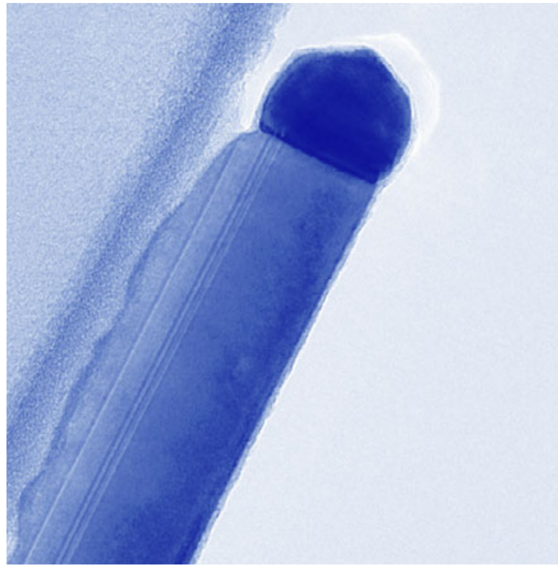

High resolution and cross-sectional transmission electron microscopy (HRTEM, XTEM) were used to characterize common defects in wurtzite GaN nanowires grown via the vapor-liquid-solid (VLS) mechanism. High resolution transmission electron microscopy showed that these nanowires contained numerous (001) stacking defects interspersed with cubic intergrowths. Using cross-sectional transmission electron microscopy, bicrystalline nanowires were discovered with two-fold rotational twin axes along their growth directions, and were concluded to grow along high index directions or vicinal to low index planes. A defect-mediated VLS growth model was used to account for the prevalence of these extended defects. Implications for nanowire growth kinetics and device behavior are discussed.

GaN is a direct gap semiconductor with a 3.39 eV band gap, and is extensively used in blue and ultraviolet light-emitting and laser diodes.[1] It is also the material of choice for high-temperature, high-voltage and high-power optoelectronic devices by virtue of its high melting temperature, high breakdown field and high saturation drift velocity. Research interest in GaN nanowires has intensified in recent years because for sufficiently thin nanowires, quantum confinement effects which enable novel applications may be observed.[2] . Proof-of-concept GaN nanowire devices have been demonstrated for photonic, optoelectronic and electronic device applications.[3-6] GaN nanowires appear to be especially attractive as low-dimensional high-power blue and ultraviolet laser light sources because it is anticipated that high optical gains and low lasing thresholds will be achievable when the nanowire diameter is smaller than the exciton radius.[7]

Unlike conventional single-crystalline GaN films grown on mismatched substrates, where threading misfit dislocations often limit device performance, dislocations are rare in GaN nanowires. Even when GaN nanowires are grown on mismatched substrates, the nanowire-substrate misfit strain can be accommodated coherently without nucleation of misfit dislocations.[8] Luminescence, normally quenched in the presence of optically active threading dislocations in GaN films,[9] is therefore comparatively enhanced in nanowires.[8] When other defects such as stacking faults are present, additional electronic states may be introduced near the band edges, which can also influence the nanowire luminescence characteristics.[10] In order to investigate the implications of extended defects for nanowire device applications, we imaged defects in GaN nanowires using high resolution (HRTEM) and cross-sectional transmission electron microscopy (XTEM).

The present work is the result of detailed observations on more than fifty nanowires from ten different synthesis experiments.

Our GaN nanowires were synthesized with the aid of AuPd as a vapor-solid-liquid (VLS) catalyst (see *Experimental* for details). At the end of each run the substrates were covered with a dense yellowish film containing the GaN nanowires. Typical VLS-grown GaN nanowires exhibited triangular cross-sections when observed end-on in scanning electron microscope (SEM) images (Fig. 1). When observed in the TEM, each of these nanowires was straight, smooth and tipped with a catalyst particle, a hallmark of the VLS process (Fig. 2a). This morphology was consistent throughout the sample and routinely reproducible. In rare growth accidents, the catalyst particle was displaced to the side of the nanowire tip (Fig. 2b) but this did not impact the overall morphology. Qualitative analysis using both x-ray energy dispersive spectroscopy (XEDS) and electron energy-loss spectroscopy (EELS) confirmed that the nanowires were GaN covered with one to a few monolayers of surface oxide, while the catalyst particles consisted of AuPd with a small amount of Ga. The GaN nanowires were heavily *n*-doped, probably by Si or O in our quartz tube growth system, and we have estimated a dopant concentration of 2×10^{19} cm^{-3} (~30 ppm) from separate transport experiments.[11] Detection of dopant concentrations is a challenge even with EELS, which has higher sensitivity for light elements than XEDS. Following Egerton,[12] we estimate minimum detectable atomic fractions on the order of 0.01-0.1% for O and 0.1-1% for Si for our EELS measurements. This upper bound on impurity levels in our GaN nanowires is entirely consistent with degenerate doping.

Using electron diffraction in the TEM, we found that most of the nanowires were grown along [120] of the wurtzite GaN structure. When the projected thicknesses through the nanowires were measured with electron energy-loss spectroscopy (EELS), the line profiles obtained were triangular and are plotted in the lower row of Fig. 2. Using cross-sectional TEM (not shown here), we observed that the growth facets on these triangular nanowires were (001), $(2\bar{1}\bar{2})$ and $(\bar{2}1\bar{2})$ polar surfaces,[13] in agreement with published data.[14]

Wurtzite GaN has a non-centrosymmetric crystal structure where the $[001]$ and $[00\bar{1}]$ c-axis directions are not related by a mirror operation. Consequently, the (001) and $(00\bar{1})$ polar surfaces have different structures and properties. It is necessary to specify explicitly the c-axis orientation (the crystal polarity) when describing the crystal structure of GaN nanowires. Most importantly, the lack of mirror symmetry along the c-axis results in asymmetric contrast in convergent beam electron diffraction (CBED) patterns along $(00l)$ lattice rows with the right choice of imaging conditions. We capitalized on this fact, and determined the thickness and polarity of the [120] nanowires by acquiring experimental CBED patterns and matching computer simulations to experiment. In the bright-field TEM image of Fig. 3a, a GaN nanowire with triangular cross-section is supported over a hole by the amorphous holey carbon film on the left. The TEM imaging geometry of the electrons (red arrows) through the nanowire (blue triangle) is shown in the inset. A CBED pattern (Fig. 3b) was recorded from the nanowire at the position marked by the red crosshair in Fig. 3a. Bloch-wave CBED simulations were then

performed and the simulation results were matched to the experimental CBED patterns. The best agreement was obtained with a 39 nm thick GaN slab imaged along [100] (Fig. 3c). In all cases, nanowires were faceted to expose the (001) polar surface along the base of the triangle. The atomically abrupt catalyst-nanowire interface also indicated that these nanowires were grown along the [120] direction via the stacking of (010) planes.

In addition, these GaN nanowires exhibited distinctive defect morphology when imaged down the $\langle 100 \rangle$ zone axes (Fig. 3a). Multiple parallel alternately bright and dark lines were observed across the width of these nanowires, creating the impression of a layered structure. These striations were planar defects that ran along the entire nanowire parallel to the (001) planes. At higher magnifications, high resolution TEM (HRTEM) images were acquired over these defected nanowire regions. Fig. 4 shows a HRTEM image of such a defected region with the $[00\bar{1}]$ apex on the right of the image. Ssimulations were run to interpret the image contrast in the HRTEM micrograph. Since the cross-sectional shape of the nanowire was known to be triangular with a wedge angle of 63.16° at the $[00\bar{1}]$ apex,[14] the local thicknesses of the nanowire were calculated and supplied to the simulation software. The simulated images are shown in boxes with the local thickness indicated. They are an excellent match to the experimental HRTEM at all except the thinnest and thickest regions. Near the middle of the image, the lattice symmetry and periodicity was different from the rest of the wurtzite GaN nanowire. Simulations showed that this region was cubic GaN imaged down [110], where the cubic {111} planes run parallel to the wurtzite (001) planes. This $(111)_{cubic}//(001)_{wurtzite}$

orientation relationship is common between cubic and hexagonal lattices, and suggests that these planar defects are stacking faults.

Analysis of the atomic structure of the cubic and wurtzite phases of GaN proved that the cubic region was formed as a result of a change in stacking from the wurtzite ABAB order to the cubic ABCABC order. The stacking order across the stacking faults is marked in Fig. 4. (001) stacking defects are known to have low defect energy and occur frequently in GaN thin film growth[15] especially when impurities are present.[16-18] These (001) stacking defects also account for the contrast striations along the lengths of the nanowires. Since these stacking faults introduce electronic levels just above the valence band maximum, they may participate in optical transitions and should be observable in GaN photoluminescence experiments.[10, 19] This suggests that photoluminescence may be used to detect the presence of stacking faults in bulk nanowire samples. Multiple stacking faults may also create quantum well-like regions of cubic GaN within the wurtzite lattice that may bind excitons and act as quench sites for luminescence.[19] We stress that (001) twins cannot be the cause of the contrast striations, since the polarity would be inverted across the twin. In addition, as crystal faceting is strongly linked to the polarity of the exposed crystal surfaces, twins in the nanowires would cause the cross-section of the nanowire to depart significantly from the simple triangular shape. No change of the crystal polarity was detected when we acquired and indexed a few CBED patterns across the width of our nanowires, and the nanowires had triangular cross-sections even in the presence of these planar defects (see Fig. 1 and 2). Therefore, the contrast striations cannot be (001) twins.

Nonetheless, we found that twinning was surprisingly common in some of our other GaN nanowire samples. Discovered in cross-sectional studies of GaN nanowires (see *Experimental* and a related work[20] for details), the cross-sections of some nanowires exhibited two-fold rotational symmetry about the growth axis (Fig. 5a). All of them exhibited distinctly different faceting and crystal habits, and though no consistent growth direction could be assigned, they appear to grow along high-index growth directions or slightly displaced (~5 mrad) from low-index ones (for example, along [174] in the CBED in Fig. 5b, verified by the simulation in Fig. 5c). We are certain of this because extraordinary care was taken to acquire these CBED patterns parallel to their growth directions (to a precision of ~1 mrad). Most importantly, the 180° rotation symmetry of the crystal facets around the center of the nanowire suggest that they contain a two-fold rotational twin axis along the growth direction and are bicrystalline. This was confirmed with CBED patterns obtained at the red crosshairs (Fig. 5b) in Fig. 5a, which were 180° rotated from those obtained at the blue crosshairs (not shown). The twin plane (composition plane) bisecting the bicrystalline nanowire can be clearly seen in the XTEM images.

An important question is why these stacking defects and specifically bicrystalline nanowires are as common as they are. First, HRTEM images of different nanowires showed that stacking defects extend along the entire lengths of the nanowires without any apparent change in the stacking order. We believe that they must play an important role in the growth process, since stacking defects are high energy sites that could serve as nuclei according to conventional theories of crystal growth.[21, 22] Second, the twin

planes in the bicrystalline nanowires were also observed to persist along the entire length of the nanowire. In rotational twins, the twin plane is not bounded by a low index crystal plane and can be considered a vicinal surface. Thus high energy lattice sites exist along the length of the twin plane and serve as crystallization nuclei. At high temperature, free vicinal surfaces will generally planarize into low index crystal facets to lower the surface energy via step-flow growth initiated at these high energy sites. However, because the twin plane is not free but connects both halves of the twinned crystal, planarization cannot occur. Consequently the twin plane persists as a continual source of crystallization nuclei along the entire length of the bicrystalline nanowire.

We propose a defect-mediated VLS growth model to qualitatively explain these observations (see Fig. 6). During the initial stages of nanowire growth, the first crystal layers that are nucleated underneath the VLS catalyst may contain planar defects. Nanowires with large numbers of stacking defects or a twinning plane (represented by vertical lines within the right-hand nanowire in Fig. 6a) expose more nucleation sites at the growing catalyst-nanowire interface than nanowires with fewer or no defects (left-hand nanowire in Fig. 6a), and therefore grow more quickly and to greater lengths (Fig. 6b). These defected nanowires then dominate the nanowire population. Conversely, this means that longer wires are expected to contain a relatively larger number of such stacking defects or a twin boundary.

The model is also compatible with our observation that specifically twin boundaries are found in bicrystalline nanowires. At first glance this observation appears to run counter to the model predictions: since a random grain boundary should contain more

high energy sites (nucleation sites) than a more symmetric twin boundary, one would conclude that bicrystalline (or polycrystalline) nanowires containing random grain boundaries should grow faster and longer than nanowires containing lower energy rotational twin boundaries. By this reasoning, rotationally twinned nanowires should be relatively uncommon, yet we encountered such nanowires in 4 out of 6 successful cross-sections from two separate synthesis runs. In fact, bicrystals with random grain boundaries expose crystal surfaces with different growth rates at the catalyst-nanowire interface (represented by different shading patterns in the left-hand nanowire of Fig. 6c), so that they eventually "grow out" the boundary when one half of the crystal overtakes the other. These nanowires then continue growth as single crystals (see left-hand nanowire in Fig. 6d). For sustained growth of a bicrystalline nanowire, the growth rates of both bicrystal halves must match in order for the boundary to persist during the VLS growth process. This constraint is best accommodated if the bicrystal is twinned along the growth axis (by a mirror or a rotational twin, see right-hand nanowire of Fig. 6c and Fig. 6d), since identical crystal facets are exposed at the growth interface under the VLS catalyst. Such a growth constraint can therefore serve as a strong "selection rule" for a small set of "allowed" bicrystal configurations.

In summary, GaN nanowires grown via the VLS growth process were characterized using TEM imaging. Nanowires were found to be mostly wurtzite GaN grown along the [120] direction. These [120] nanowires always exhibited a distinctive triangular cross-section, and contained numerous (001) stacking defects, likely due to the presence of impurities. Sometimes cubic GaN regions were observed within the predominantly GaN

nanowires due to changes in the stacking order. These growth defects were presumed to be linked to the nanowire growth kinetics, and a defect-mediated VLS growth model was proposed that explained the prevalence of these defected nanowires. In addition, bicrystalline nanowires were discovered with two-fold rotational twin axes along their growth directions, and were concluded to grow along high index directions or slightly tilted away from low index ones. The presence of these bicrystalline nanowires was also explained successfully within the defect-mediated VLS growth model when an additional growth constraint was added.

The ubiquity of these extended defects in our samples suggests that they may also be common in samples of other researchers grown under similar conditions or containing similar impurities. This is especially true if our defect-mediated VLS growth model is correct, since it predicts that defected nanowires tend to grow faster and longer and eventually dominate the population. These defects are expected to impact nanowire luminescence behavior considerably, but detailed studies of defect optical properties have yet to be performed. Additionally, to the best of our knowledge, no work has been done to establish connections between growth method, impurity content and luminescence quantum yield. We believe that these questions can be answered when single nanowire optoelectronic or luminescence measurements are coupled with detailed TEM characterization on the same nanowire.

EXPERIMENTAL

The *n*-type GaN nanowires used for this work were synthesized by thermal vaporization of Ga_2O_3 under NH_3 atmosphere using a sputter-deposited AuPd film as the vapor-liquid-solid (VLS) catalyst.[23] The AuPd films were coated on Si chip substrates that were held at 900°C for the duration of each synthesis run. After growth, the GaN nanowires were dispersed onto holey carbon coated Cu grids for HRTEM analysis. To do this, we pressed each Cu grid gently onto the growth substrates containing the as-grown nanowires. Using this "dry transfer" we were able to avoid solvent contamination of the nanowire surfaces. For XTEM experiments, the GaN nanowires were dispersed onto Si chips covered with 100 nm of Si_3N_4 or SiO_2, and cross-sections of these nanowires were then obtained inside a focused ion beam (FIB). TEM observations were performed with a 197 keV TEM (JEOL 2010F) equipped with x-ray energy dispersive spectroscopy (XEDS, PGT-IMIX) and EELS (Gatan Imaging Filter) spectrometers. The cross-sections were carefully tilted to image them along the nanowire growth direction.

The cross-sections were produced by the lift-out technique, which has been described by Giannuzzi *et al*,[24] while while another application of our methodology has been published recently.[11] First, a region of interest was selected upon which a protective "capping layer" of Pt is deposited using the electron beam. This layer serves to protect the target region from inadvertent milling by the ion beam. Next, trenches on either side of the target region were milled away using the ion beam to expose a ~1 μm thick slab. This slab was then gripped using a FIB micromanipulator and cut free from the substrate using the ion beam. The micromanipulator controls were used to distance the slab from the substrate, and the slab was thinned to electron transparency with progressively

smaller ion beam currents. Cross-sections with thicknesses of ~100-200 nm were obtained, although the exact thickness was difficult to control. Electron energy-loss spectroscopy (EELS) measurements of cross-sectional thickness in regions of identical composition showed that the surfaces were very flat, and the standard deviation of the thickness variations never exceeded 3%.

FIGURE CAPTIONS

Fig. 1. SEM image revealing triangular cross-sections of GaN nanowires at broken ends. The cross-section is isosceles, not equilateral, due to the wurtzite crystal structure with non-ideal c/a ratio.

Fig. 2. (a) and (b) Bright-field STEM images of typical VLS-grown GaN nanowires, taken along two different low index directions. The VLS catalyst particle is always found at one end of the nanowire, usually at the tip, although it may sometimes be found displaced to the side with otherwise no impact on nanowire morphology. (c) and (d) Typical projected thickness line profiles measured by EELS, taken across the dashed lines in (a) and (b) respectively.

Fig. 3. (a) Bright-field TEM image of a [120] GaN nanowire imaged down [100]. Key lattice directions and planes have been labeled. A crosshair marks the approximate location at which the CBED was recorded. The inset indicates the TEM imaging geometry of the electrons (arrows) through the triangular nanowire (triangle). (b) Experimental CBED obtained from the nanowire along [100]. (c) Bloch-wave CBED simulation along [100] for a 39 nm thick GaN slab using a convergence semiangle of 1.97 mrad. The zone axis has been displaced about 0.7 mrad towards $[0\bar{1}\bar{1}]$.

Fig. 4. Experimental HRTEM image of a [120] nanowire imaged down the $[\bar{1}00]$ direction, with the $[00\bar{1}]$ direction marked. Wurtzite and cubic GaN regions are clearly separated by planar (001) stacking defects, which run vertically down the image. The

boxes contain simulated HRTEM images at a defocus Δf = -22 nm, each labeled with the specimen thickness. The stacking order near the cubic GaN region is shown. A slight sample tilt on the order of 1 mrad has been applied towards $[011]$ to improve the match.

Fig. 5. (a) Bright-field XTEM image of a bicrystalline GaN nanowire cross-section imaged down $[174]$. (b) Contrast-enhanced experimental CBED obtained from the nanowire along $[174]$ at the red crosshair, which is 180° rotated from the CBED taken at the blue crosshair (not shown). (c) Contrast-enhanced Bloch-wave CBED simulation along $[174]$ for a 240 nm thick GaN slab using a convergence semiangle of 6.77 mrad. The zone axis has been displaced by about 3 mrad towards $[\bar{1}3\bar{5}]$. The dark lines present in the experimental CBED were not simulated.

Fig. 6. The defect-mediated VLS growth model. (a) During the initial stages of nanowire growth, crystal layers nucleated from the VLS catalyst may contain planar defects. (b) Nanowires with more planar defects expose more nucleation sites at the growth interface and grow faster and longer. (c) Initial crystal layers could also be bicrystalline, with a random grain boundary or a symmetric twin boundary. (d) The growth rates of each half are matched only for twinned nanowires that expose the same crystal plane at the growth interface, so random grain boundaries do not persist.

FIG. 1. D. Tham *et. al.*

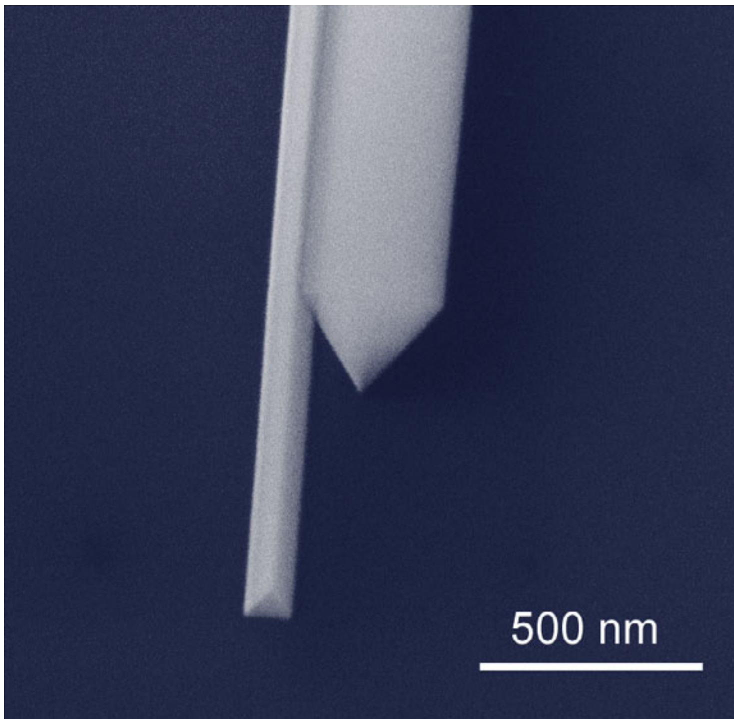

FIG. 2. D. Tham *et. al.*

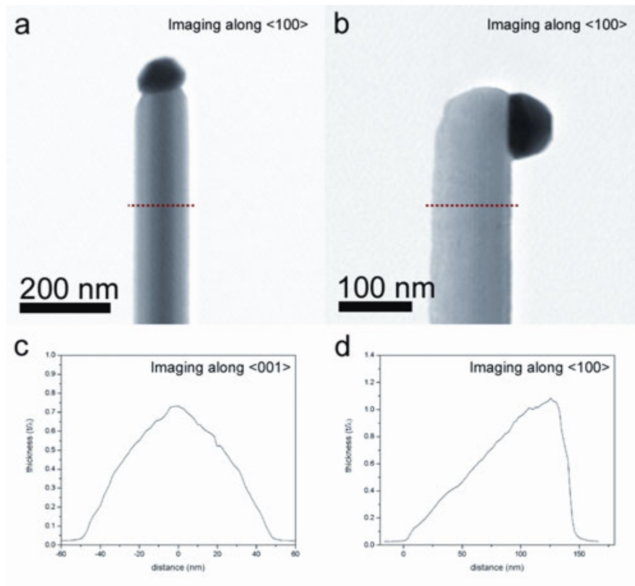

FIG. 3. D. Tham *et. al.*

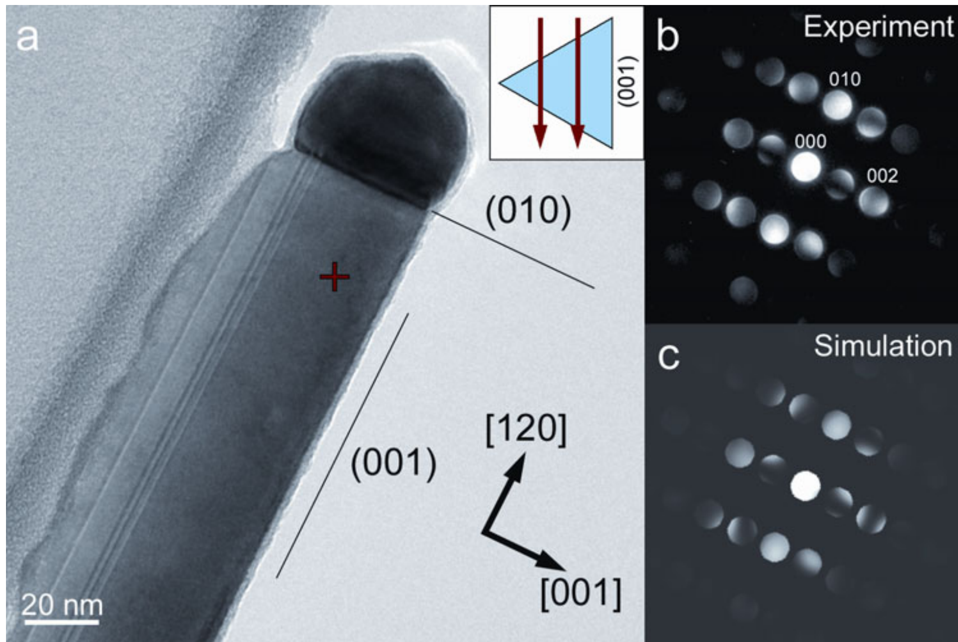

FIG. 4. D. Tham *et. al.*

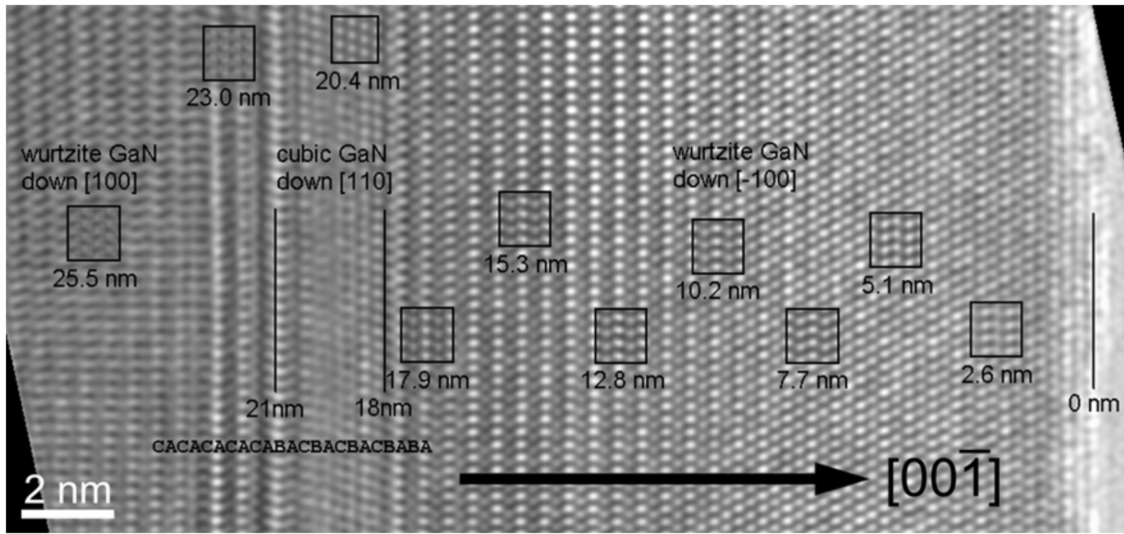

FIG. 5. D. Tham *et. al.*

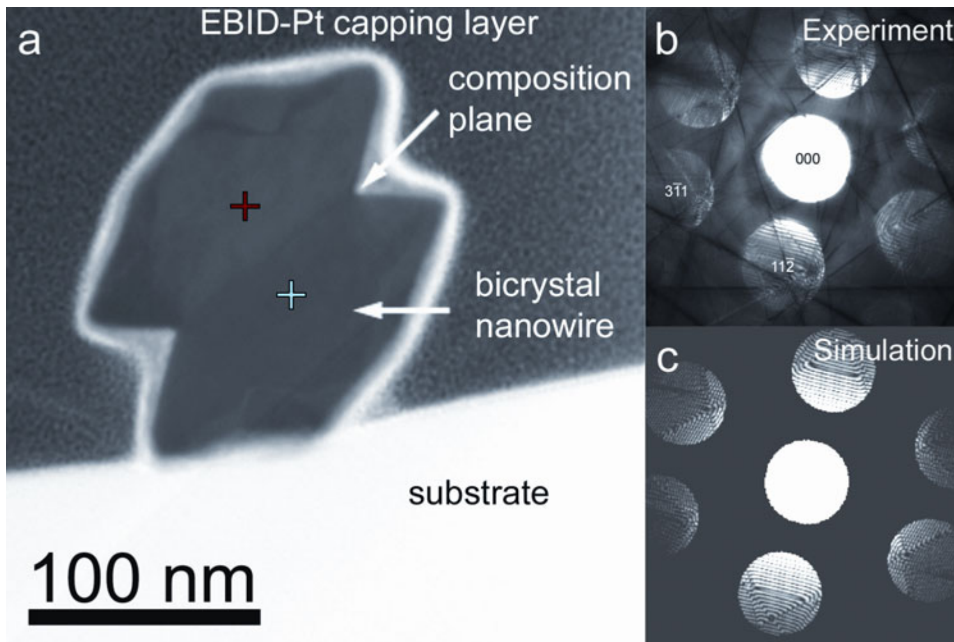

FIG. 6. D. Tham *et. al.*

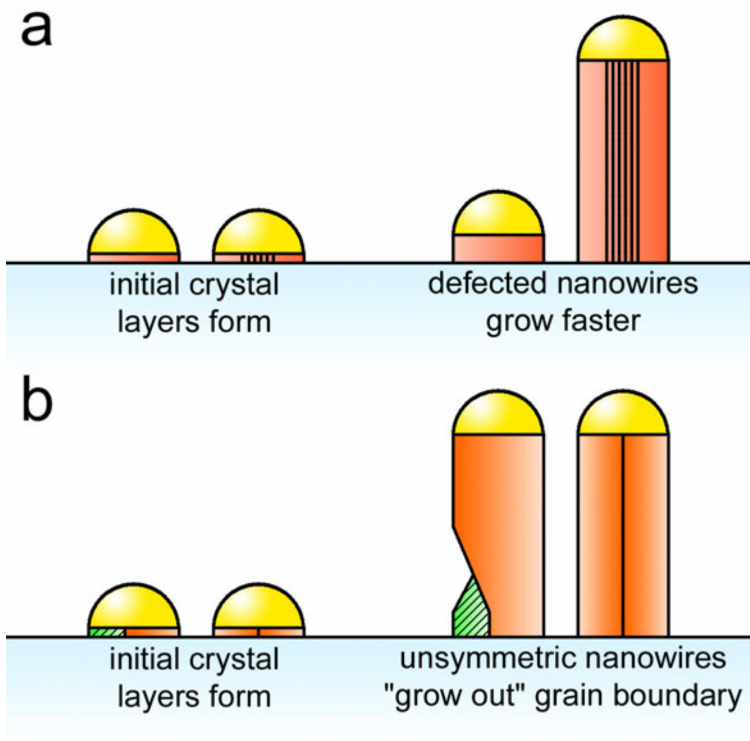

REFERENCES

[1] S. Nakamura, S. Pearton, G. Fasol, *The Blue Laser Diode*, Springer, 2000, p. 368.
[2] H. Yu, J. Li, R. A. Loomis, L.-W. Wang, W. E. Buhro, *Nature Mater.* **2003**, *2*, 517-520.
[3] Y. Huang, C. M. Lieber, *Pure Applied Chemistry* **2004**, *76*, 2051-2068.
[4] F. Qian, Y. Li, S. Gradecak, D. Wang, C. J. Barrelet, C. M. Lieber, *Nano Lett.* **2004**, *4*, 1975-1979.
[5] P. Yang, *MRS Bull.* **2005**, *30*, 85-91.
[6] Y. Huang, X. Duan, Y. Cui, C. M. Lieber, *Nano Lett.* **2002**, *2*, 101-104.
[7] T. Uenoyama, *Phys. Rev. B: Condens. Matter* **1995**, *51*, 10228-10231.
[8] Y. Inoue, T. Hoshino, S. Takeda, K. Ishino, A. Ishida, H. Fujiyasu, *Appl. Phys. Lett.* **2004**, *85*, 2340-2342.
[9] Y. Xin, S. J. Pennycook, N. D. Browning, P. D. Nellist, S. Sivananthan, F. Omnès, B. Beaumont, J. P. Faurie, P. Gibart, *Appl. Phys. Lett.* **1998**, *72*, 2680-2682.
[10] Z. Z. Bandić, T. C. McGill, Z. Ikonić, *Phys. Rev. B: Condens. Matter* **1997**, *56*, 3564-3566.
[11] C. Y. Nam, D. Tham, J. E. Fischer, *Nano Lett.* **2005**, *5*, 2029-2033.
[12] R. F. Egerton, *Electron energy-loss spectroscopy in the electron microscope*, Plenum Press, 1996, p. 500.
[13] C. Y. Nam, P. Jaroenapibal, D. Tham, J. E. Fischer, D. E. Luzzi, S. Evoy, *Nano Lett.* **2005**, (in press).
[14] T. Kuykendall, P. Pauzauskie, S. Lee, Y. Zhang, J. Goldberger, P. Yang, *Nano Lett.* **2003**, *3*, 1063-1066.
[15] X. H. Wu, L. M. Brown, D. Kapolnek, S. Keller, B. Keller, S. P. DenBaars, J. S. Speck, *J. Appl. Phys.* **1996**, *80*, 3228-3237.
[16] E. Monroy, M. Hermann, E. Sarigiannidou, T. Andreev, P. Holliger, S. Monnoye, H. Mank, B. Daudin, M. Eickhoff, *J. Appl. Phys.* **2004**, *96*, 3709-3715.
[17] J. A. Chisholm, P. D. Bristowe, *J. Cryst. Growth* **2001**, *230*.
[18] L. Mancera, J. A. Rodríguez, N. Takeuchi, *Phys. Status Solidi B* **2004**, *241*, 2424-2428.
[19] C. Stampfl, C. G. Van de Walle, *Phys. Rev. B: Condens. Matter* **1998**, *57*, R15052.
[20] D. Tham, C. Y. Nam, J. E. Fischer, *Adv. Mater.* **2005**, (in press).
[21] R.-F. Xiao, J. I. D. Alexander, F. Rosenberger, *Phys. Rev. A* **1991**, *43*, 2977-2992.
[22] D. A. Porter, K. E. Easterling, *Phase transformations in metals and alloys*, CRC Press, 1992, p. 514.
[23] C. Y. Nam, D. Tham, J. E. Fischer, *Appl. Phys. Lett.* **2004**, *85*, 5676-5678.
[24] L. A. Giannuzzi, J. L. Drown, S. R. Brown, R. B. Irwin, F. A. Stevie, *Microsc. Res. Technique* **1998**, *41*, 285-290.